Characterization of Two Oxidatively Modified Phospholipids in Mixed Monolayers with DPPC

Karen Sabatini,*† Juha-Pekka Mattila,† Francesco M. Megli,* and Paavo K. J. Kinnunen†
*Dipartimento di Biochimica e Biologia Molecolare, Università di Bari, Centro di Studio sui Mitocondri e Metabolismo Energetico—CNR, Bari, Italy; and †Helsinki Biophysics and Biomembrane Group, Medical Biochemistry, Institute of Biomedicine, University of Helsinki, Helsinki, Finland

ABSTRACT The properties of two oxidatively modified phospholipids viz. 1-palmitoyl-2-(9′-oxo-nonanoyl)-*sn*-glycero-3-phosphocholine (PoxnoPC) and 1-palmitoyl-2-azelaoyl-*sn*-glycero-3-phosphocholine (PazePC), were investigated using a Langmuir balance, recording force-area (π-A) isotherms and surface potential ψ. In mixed monolayers with 1,2-dipalmitoyl-*sn*-glycero-3-phosphocholine (DPPC) a progressive disappearance of the liquid expanded-liquid condensed transition and film expansion was observed with increasing content of the oxidized phospholipids. The above is in agreement with fluorescence microscopy of the monolayers, which revealed an increase in the liquid expanded region of DPPC monolayers. At a critical pressure $\pi_s \sim 42$ mN/m both Poxo- and PazePC induced a deflection in the π-A isotherms, which could be rationalized in terms of reorientation of the oxidatively modified acyl chains into aqueous phase (adaptation of the so-called extended conformation), followed upon further film compression by solubilization of the oxidized phospholipids into the aqueous phase. Surface potential displayed a discontinuity at the same value of area/molecule, corresponding to the loss of the oxidized phospholipids from the monolayers. Our data support the view that lipid oxidation modifies both the small-scale structural dynamics of biological membranes as well as their more macroscopic lateral organization. Accordingly, oxidatively modified lipids can be expected to influence the organization and functions of membrane associated proteins.

INTRODUCTION

Biological membranes are centrally involved in the control and execution of a great variety of cellular processes, thus requiring the maintenance of their proper structure and function (1–4). The structural core of all biomembranes is provided by the lipid bilayer. The fluid mosaic model (5) described biomembranes mainly as a diffusion barrier and a structural matrix embedding the active molecules, peripheral and integral membrane proteins, and covalently linked complex carbohydrates. Yet, it has become evident that biomembranes possess a considerable degree of static and dynamic heterogeneity because of i), the large number of different lipid species; and ii), their liquid crystalline nature (1,6–9). Furthermore, the lateral organization and the thermodynamic state of biomembranes determined by their lipids have been suggested to be correlated to the physiological functional states of cells (1), determining, e.g., protein-lipid interactions, further controlling the activity of membrane associated enzymes, for instance (2,3,10–16). Accordingly, perturbing the bilayer structure leads to modifications of membrane properties, as well as alterations and loss of both integral (17,18) and peripheral (19,20) protein-lipid interactions and, subsequently, changes in a variety of biological processes (21–25).

Reactive oxygen species (ROS) are produced by cellular metabolism, mitochondrial respiration in particular, as well as in processes such as inflammation and phagocytosis of virus- or bacteria-infected cells (26,27). The formation of ROS is induced also by ultraviolet and ionic irradiation of cells (28,29). ROS overproduction damages cellular macromolecules, above all lipids, and the latter have been suggested also to be the targets for the above radiations (30). Extensive evidence supports the notion that lipid peroxidation is centrally involved in degenerative, age-related diseases such as Parkinson's and Alzheimer's disease (21,31–34), as well as cardiac arrhythmia, hypertension, inflammatory diseases (21,31,35), schizophrenia (36), and cancer (37–40). Yet, in spite of their obvious relevance to the understanding of the molecular basis of the above pathological conditions the exact mechanisms of action of oxidized lipid species have remained elusive. It has been proposed that membrane damage after oxidative attack involves impairment of ion transport mechanisms (41) and modification of the function of membrane proteins (1,22). To this end, similarly to lipids in general, also oxidized lipid species can elicit their cellular level effects by two principally different mechanisms, viz. by influencing and perturbing lipid-protein interactions via liganding to specific proteins, as well as by modifying the membrane bulk physical properties (1). The latter mechanism is likely to act high in the hierarchy of cellular control mechanisms, integrating entire metabolic pathways in the various organelles (42).

Oxidative damage of the acyl chains causes loss of double bonds, chain shortening, and the introduction of hydroperoxy

Submitted December 21, 2005, and accepted for publication March 6, 2006.

Address reprint requests to Paavo K. J. Kinnunen, Helsinki Biophysics and Biomembrane Group, Medical Biochemistry, Institute of Biomedicine, PO Box 63 (Haartmaninkatu 8), FIN-00014, University of Helsinki, Finland. Fax: 358-0-191-25444; E-mail: paavo.kinnunen@helsinki.fi.

0006-3495/06/06/4488/12 $2.00

doi: 10.1529/biophysj.105.080176

groups and is thus expected to affect the structural characteristics and dynamics of lipid bilayers (43–45), such as decrease in phospholipid acyl chain order, evident as loss of anisotropy in the EPR spectra of spin-labeled oriented planar layers (46–48). Importantly, the above could be demonstrated also for phospholipids from isolated rat liver mitochondria maintained in respiration state IV in vitro (49), as well as for liver mitochondrial phospholipids from rats treated with carbon tetrachloride (50). It is also relevant to note that lipid peroxidation is a chain reaction and leads to a facile propagation and spreading of free radical reactions in the affected tissues, causing under pathological conditions accumulation of oxidized lipids (51). Because of the obvious importance of understanding changes in the biophysical properties of lipid bilayers imposed by peroxidized lipids, we characterized by Langmuir balance the effects of two oxidatively modified phospholipid species on the monolayer properties of 1,2-dipalmitoyl-*sn*-glycero-3-phosphocholine (DPPC). The two lipids used in the present study were 1-palmitoyl-2-(9′-oxo-nonanoyl)-*sn*-glycero-3-phosphocholine and 1-palmitoyl-2-azelaoyl-*sn*-glycero-3-phosphocholine (PoxnoPC and PazePC, respectively, Fig. 1). Importantly, their availability in pure form allows us to evaluate the contribution of individual oxidized lipid species on the measured parameters. We investigated lipid-lipid interactions by recording force-area (π-A) isotherms and calculated from these data the interfacial elastic moduli of area compressibility (C_s^{-1}), providing an indicator for changes in the structure of the film (52). Information on the electric properties of the film was obtained from the measurement of surface dipole potential ψ (53). The lateral organization of the mixed monolayers was investigated by fluorescence microscopy.

MATERIALS AND METHODS

Materials

PoxnoPC, PazePC, and 1-palmitoyl-2-(N-4-nitrobenz-2-oxa-1,3-diazol)aminocaproyl-*sn*-glycero-3-phosphocholine (NBD-PC) were from Avanti Polar Lipids (Alabaster, AL). 1,2-Dipalmitoyl-*sn*-glycero-3-phosphocholine (DPPC), NaCl, Hepes, and EDTA were from Sigma (St. Louis, MO). The purity of the above lipids was verified by thin layer chromatography on silicic acid coated plates (Merck, Rahway, NJ), using chloroform/methanol/water/ammonia (65:20:2:2, v/v) as the eluent. No impurities were detected upon examination of the plates after iodine staining. Concentrations of DPPC, PoxnoPC, and PazePC were determined gravimetrically using a high-precision electrobalance (Cahn Instruments, Cerritos, CA) and the concentration of NBD-PC was determined spectrophotometrically, using the molar extinction coefficient $\varepsilon = 21{,}000\ \mathrm{cm}^{-1}$ at 465 nm. Stock solutions of the lipids were prepared in chloroform and stored at −20°C. Freshly deionized filtered water (Milli RO/Milli Q, Millipore, Jaffrey, NH) was used in all experiments.

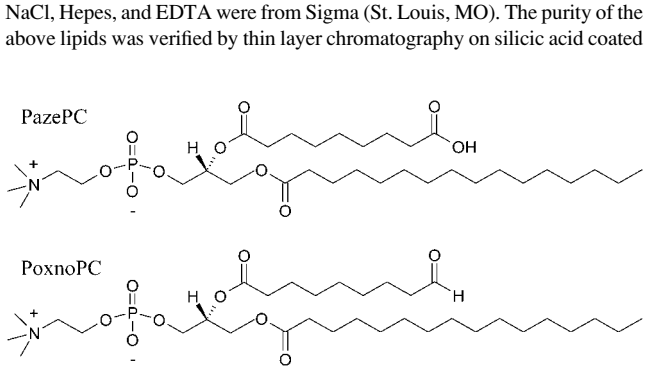

FIGURE 1 Chemical structures of the two oxidatively modified phospholipids used: (*A*) 1-palmitoyl-2-(9′-oxo-nonanoyl)-*sn*-glycero-3-phosphocholine (PoxnoPC) and (*B*) 1-palmitoyl-2-azelaoyl-*sn*-glycero-3-phosphocholine (PazePC).

Monolayer measurements

A computer-controlled Langmuir type film balance (μTrough XL, Kibron, Helsinki, Finland) equipped with a Precision Plus trough was used to simultaneously measure π-A and $\Delta\psi$-A isotherms, using the embedded features of the control software (FilmWare 3.52, Kibron). The indicated lipid mixtures were made in chloroform and were spread in this solvent onto the air-aqueous phase (15 mM NaCl) interface with a Hamilton microsyringe. This subphase was employed since the presence of salt decreases noise in the surface potential measurements. Compression isotherms recorded on 20 mM Hepes, 0.1 mM EDTA, pH 7.4 were indistinguishable from these reported here (data not shown). Total surface area of the trough is 120 cm^2 and the volume of the subphase is 20 ml. After 5 min equilibration (to ensure evaporation of the solvent), the film compression was started using two symmetrically moving barriers. Compression rate was in all measurements 4 $\mathrm{Å}^2$/chain/min, so as to allow for the reorientation and relaxation of the lipids in the course of the compression. Surface pressure (π) was monitored with a metal alloy probe hanging from a high precision microbalance (KBN 315, Kibron) connected to a computer and is defined as

$$\pi = \gamma_o - \gamma, \tag{1}$$

where γ_o is the surface tension of the air/buffer interface and γ is the value for surface tension in the presence of a lipid monolayer compressed to varying packing densities. Monolayer dipole potential ψ (53) was measured using the vibrating plate method (μSpot, Kibron). All the isotherms were recorded at ambient temperature and were repeated at least twice to ensure reproducibility.

Analysis of isotherms

Phase transitions were identified using derivatives of surface pressure with respect to area (54). The value for monolayer isothermal compressibilities (C_S) for the indicated film compositions at the given surface pressure (π) was obtained from π-A data using

$$C_S = (-1/A_\pi)\times(dA/d\pi)_T, \tag{2}$$

where A_π is the area per molecule at the indicated surface pressure π. To identify the phase transition points we further analyzed our data in terms of the reciprocal isothermal compressibility (C_s^{-1}) as discussed previously (55). Accordingly, the higher the value for C_S^{-1}, the lower the interfacial elasticity.

The collected $\Delta\psi$ versus A data were analyzed in terms of $\mu\perp$, the component of the monolayer dipole moment vector perpendicular to the monolayer plane. The values for $\mu\perp$ were obtained essentially as described by Brockman (53). In short, $\Delta\psi$ was plotted against $1/A_m$ and subsequently the linear regions of curve were fitted by equation

$$\Delta\psi = \Delta\psi_0 + 37.70\mu\perp\times 1/A_m, \tag{3}$$

to give an estimate of molecular dipole moment $\mu\perp$.

Fluorescence microscopy

Lateral organization of mixed monolayers of DPPC and either PoxnoPC or PazePC was observed by fluorescence microscopy whereas compressing the indicated films in the above described instrument to the given values of π. The trough (μTroughS) was mounted on the stage of an inverted microscope (Zeiss

IM-35, Jena, Germany) and the quartz-glass window in the bottom of the trough was positioned over an extra-long working distance 20× objective (Nikon, Tokyo, Japan). A 450–490 nm bandpass filter was used for excitation and a 520-nm longpass filter for emission. Images were viewed with a Peltier-cooled 12-bit digital camera (C4742-95, Hamamatsu Photonic, Hamamatsu, Japan) interfaced to a computer and running image-processing software provided by the camera manufacturer (HiPic, 4.2.0). NBD-PC ($X = 0.02$) was included in the indicated lipid mixtures as a fluorescent probe (56). After equilibration the monolayers were compressed at a rate of 2 Å^2/chain/min by two symmetrically moving barriers. All measurements were carried out at ambient temperature of 24 ± 1°C and were repeated at least twice. The percentages of the monolayer in fluid and solid phases at given values of surface pressure were calculated from the fluorescence microscopy images using the program ImageJ.

RESULTS

π-A isotherms for PoxnoPC/DPPC and PazePC/DPPC monolayers

Compression isotherms (Fig. 2, *A* and *B*) were first recorded for binary mixtures of the aldehyde group bearing PoxnoPC (Fig. 1) and DPPC. Isotherms for the latter lipid were in keeping with the behavior reported previously, with clearly discernible liquid-expanded to liquid-condensed (LE→LC) phase transition (57). Data for PoxnoPC/DPPC monolayers reveal several interesting features (Fig. 2 *A*). First, increasing X_{PoxnoPC} abolishes the LE-LC coexistence region in a progressive manner, with nearly complete disappearance at $X_{\mathrm{PoxnoPC}} = 0.40$. Yet, a discontinuity indicative of the main phase transition is still evident at $\pi \approx 20$ mN/m. This behavior suggests the films with $X_{\mathrm{PoxnoPC}} \geq 0.40$ to be predominantly in the liquid expanded state. The second interesting feature of the isotherms is the presence above $\pi =$ 40 mN/m of another transition, which becomes more pronounced with increasing X_{PoxnoPC}. Isobars of mean molecular area $\bar{A}$ versus X_{PoxnoPC} at surface pressures of 5, 10, 20, 40, and 50 mN/m were constructed (Fig. 2 *C*). At surface pressures of 5 and 20 mN/m the presence of PoxnoPC led to a slight expansion of the monolayer, whereas at 10 mN/m the expansion was more pronounced. In contrast, at surface pressure of 50 mN/m, i.e., above the transition at ~42–44 mN/m, PoxnoPC caused film condensation. However, analysis of these data revealed this condensation to be apparent only, with π approaching 0 upon $X_{\mathrm{PoxnoPC}} \rightarrow 1.0$. Accordingly, we may conclude PoxnoPC to dissolve from the monolayer into the aqueous subphase. This process appears to follow first-order kinetics, with a sharp inflection point in π-A isotherms, denoted as π_s and defined as the critical pressure for the dissolving of the oxidized lipids from the films into the aqueous phase. To this end, micelle formation in highly oxidized phospholipid mixtures has been suggested on the basis gel exclusion chromatography (58).

We then proceeded to study PazePC, which upon deprotonation of its carboxyl moiety bears a negative charge (Fig. 1). Similarly to PoxnoPC π versus A isotherms of DPPC/PazePC films reveal the disappearance of the LE→LC transition (Fig. 2 *B*). Yet, compared to PoxnoPC the curves for PazePC lift-off earlier (i.e., at lower area/molecule values) and a more pronounced shift of the curves to the right (larger area/molecule values) is evident at low pressures (Fig. 2 *B*) and already at $X_{\mathrm{PazePC}} = 0.10$, as shown also by the $\bar{A}$ versus X_{PazePC} data at 5, 10, 20, 40, and 50 mN/m (Fig. 2 *D*), showing the pressure and composition dependent expanding and condensing effects of PazePC in DPPC monolayers. For PazePC film expansion is pronounced already at X_{PazePC} from 0.10 to 0.15. Similarly to PoxnoPC a break in the compression isotherms is seen for PazePC containing films at surface pressures π_s of ~40 to 42 mN/m, also showing loss of this oxidized lipid from the binary phospholipid monolayer into the aqueous phase.

Interfacial elastic moduli of area compressibility of PoxnoPC/DPPC and PazePC/DPPC films

To gain further insight into the structural characteristics of the oxPL/DPPC monolayers, the above compression isotherms were analyzed in terms of their compressibility modulus C_s^{-1} as a function of π and X_{oxPL} (Fig. 2, *E* and *F*). Increasing X_{oxPL} dramatically decreased C_s^{-1} for both oxidized phospholipid species, revealing augmented elasticity of the films. Compressibility data also reveal the phase transition of DPPC and the high-pressure inflection point in π-A isotherms observed for films with oxPLs, the minima in C_s^{-1} coinciding with the critical pressure π_s at surface pressures of ~42–44 and 40–42 mN/m for PoxnoPC and PazePC, respectively (Fig. 2, *E* and *F*). The depicted graphs also illustrate the differences in compression isotherms for PazePC and PoxnoPC after the high-pressure inflection. The shapes of π versus C_s^{-1} curves in the vicinity of the new transition are different for the two oxPLs. For PazePC there is a decrease of the first shoulder and an increase of the second one, whereas for PoxnoPC a decrease of both shoulders is evident both below and above π_s ~42 mN/m. In both cases the first shoulder appears close to the collapse pressure of pure oxidized lipid and after the completion of the transition the values for C_s^{-1} equal those for DPPC. C_s^{-1} versus X_{oxPL} data at surface pressures from 5 to 50 mN/m were constructed to better demonstrate the changes in film compressibility modulus with varying X_{oxPL} (Fig. 2, *G* and *H*). At 5 mN/m, the behaviors of PoxnoPC/DPPC and PazePC/DPPC films were almost identical. In contrast, at 40 mN/m the compressibility of PazePC/DPPC monolayers exceeded that of PoxnoPC/DPPC (i.e., the value of C_s^{-1} for PazePC/DPPC is lower than for PoxnoPC/DPPC), for all mole fractions studied. Further, at 40 mN/m the value of C_s^{-1} for PazePC/DPPC showed a local minimum at $X_{\mathrm{PazePC}} = 0.25$.

Surface potential-area ($\Delta\psi$-A) isotherms for oxPL/DPPC films

Taking into account the nature of the monolayers containing oxPLs one readily anticipates alterations in the monolayer dipole potential (53). Accordingly, surface potential-area isotherms for both PoxnoPC/DPPC and PazePC/DPPC monolayers were measured to further investigate the effects of these oxPLs on membrane properties (Fig. 3, *A* and *B*). A

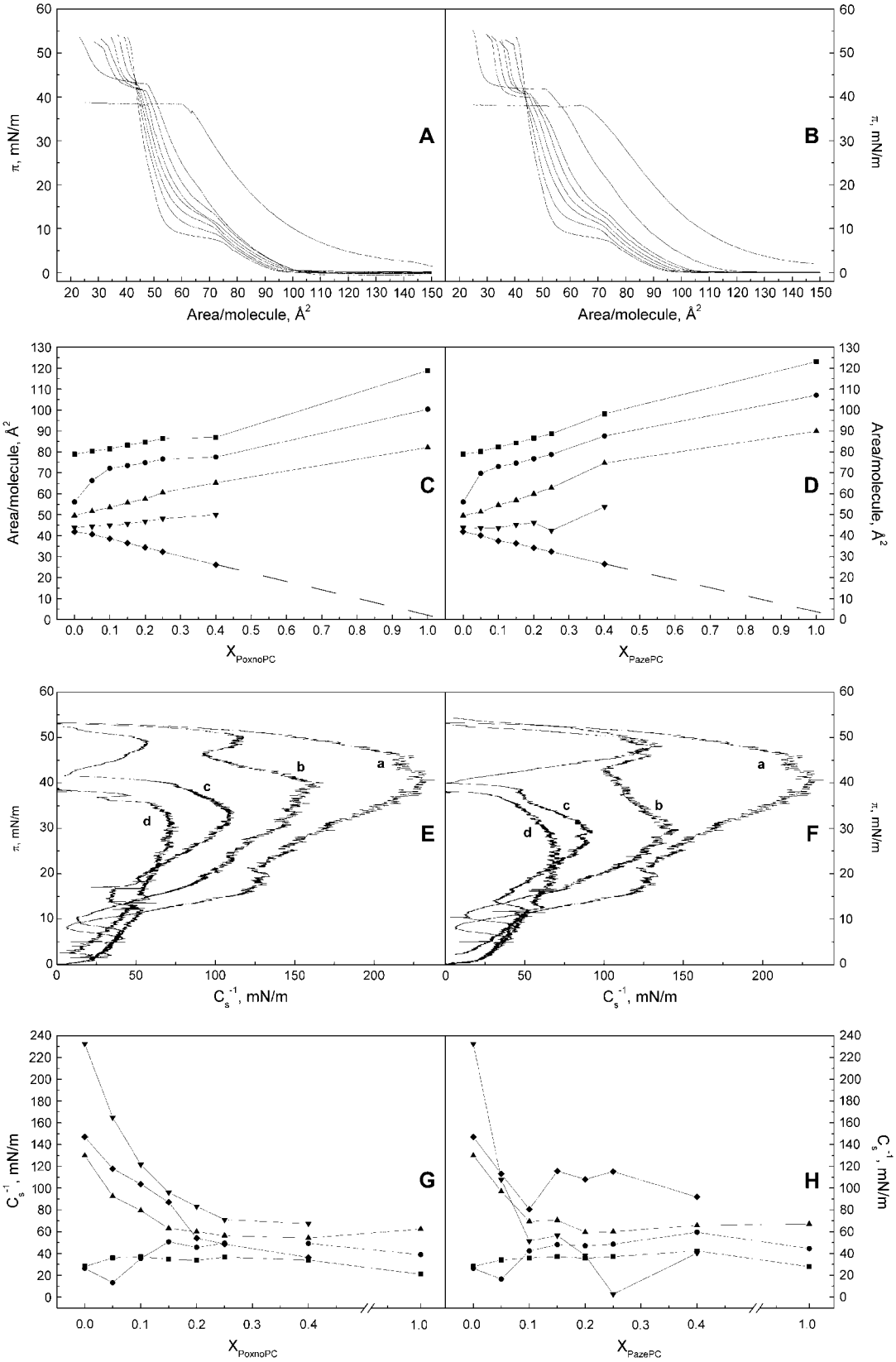

FIGURE 2. Representative compression isotherms for PoxnoPC (*A*) and PazePC (*B*) in mixed monolayers with DPPC, the mol fraction *X* of the oxidized phospholipid (X_{oxPL}) species increasing from left to right as 0.0, 0.05, 0.1, 0.15, 0.2, 0.25, 0.4, and 1.0. The given lipid mixtures were spread onto 15 mM NaCl at ambient temperature (~24°C). After 4 min of equilibration the films were compressed at a rate of 4 Å^2/molecule/min. Panels *C* and *D* illustrate variations in

shoulder at the same A/molecule corresponding to the break in π-A data at ~40 mN/m is observed for both oxPLs in DPPC, this shoulder becoming more pronounced with increasing X_{PoxnoPC} (Fig. 3 *A*). For mixed monolayers of PazePC a shoulder similar to that for PoxnoPC/DPPC films is observed (Fig. 3 *B*). Yet, the shoulder for PazePC is broader and occurs at higher mean molecular areas. To gain more insight into the differences between the two oxPLs, we constructed ψ versus X_{oxPL} isobars at 5, 10, 20, 40, and 50 mN/m (Fig. 3, *C* and *D*). Increase in X_{oxPL} decreased ψ, as compared to neat DPPC. The decrement due to PazePC (~100 mV for pure PazePC at $\pi = 5$ mN/m) was more pronounced than that due to PoxnoPC (~45 mV for pure PoxnoPC at $\pi = 5$ mN/m). Although these are considerable force fields as such, also the impact of the difference in the chemical structures is of interest with a difference of ~55 mV between PoxnoPC and PazePC at 5 mN/m (Fig. 3, *C* and *D*), the former bearing an aldehyde and the latter a carboxylic function. Finally, we also constructed ψ versus X_{oxPL} isochores at 40, 45, 50, 55, 60, 70, and 80 Å^2/molecule (Fig. 3, *E* and *F*), which demonstrate a decrement in ψ with increasing X_{oxPL}. Interestingly, the value for $\Delta\psi$ of pure PazePC and PoxnoPC was independent of the mean molecular area, indicating a packing density dependent reorientation of the component of dipole moment vector perpendicular to the monolayer plane $\mu\perp$, yielding nearly constant surface dipole potential during film compression. To better illustrate this feature values for $\mu\perp$ were calculated by fitting Eq. 3 to the linear parts of $\Delta\psi$ versus $1/A$ for the data in the liquid expanded phase (between ~75–90 Å^2/molecule) and regions between 61–65 and 40–45 Å^2/molecule. Only modest changes in $\mu\perp$ are apparent for both PoxnoPC and PazePC with increasing X_{oxPL} in the liquid expanded phase (Fig. 3, *G* and *H*). Instead, for the range 61–65 Å^2/molecule there is a drastic increase in $\mu\perp$ at $X_{\mathrm{oxPL}} = 0.1$–0.25 when compared to neat DPPC. At $X_{\mathrm{oxPL}} = 1.0$ the value of $\mu\perp$ approaches zero indicating the dipole moment vector to be oriented parallel to the monolayer surface or the oxidized phospholipid dissolving from the film into the aqueous subphase. Essentially similar behavior is observed for the range of A varying between 40 and 45 Å^2/molecule, however, the increase in $\mu\perp$ between X_{oxPL} from 0.1 to 0.25 is less pronounced.

Fluorescence microscopy of oxPL/DPPC monolayers

The impact of the oxPLs on the two-phase region of mixed films with DPPC was analyzed by fluorescence microscopy (56), visualizing the lateral distribution of the LE phase favoring fluorescent lipid analog, NBD-PC ($X = 0.02$). DPPC in the LE-LC coexistence region reveals the presence of nonfluorescent solid domains in a continuous fluid and fluorescent phase (Fig. 4). The appearance of the solid domains coincided with the onset of the LE→LC transition. The condensed domains appear to be randomly arrayed and are observed to diffuse in the plane of the monolayer due to Brownian motion. However, they rarely come into contact indicating that the domains repel each other at short distances (59,60). Upon further compression of DPPC films, the solid phase domains grow in size whereas their number decreases slightly at the expense of the fluid phase (Fig. 5). At $\pi = 40$ mN/m bright clusters of the fluorescent probe become evident, together with dark areas. Interestingly, these two domains are separated by a continuous gray area, with an apparent gradient of fluorescence intensity. With further increase of π to 50 mN/m the intermediate phase disappears and a two-phase region is seen. The presence of the two oxPLs causes drastic differences both in the size and shape of the solid condensed phase and for both PoxnoPC and PazePC the solid domains first appear at 9–10 mN/m for $X_{\mathrm{oxPL}} = 0.10$ and 0.20 (Fig. 3). At $X_{\mathrm{oxPL}} = 0.40$ no indications of phase separation at $\pi < 16$ mN/m were seen (Fig. 3), in agreement with the presence of the phase transition at ~20 mN/m for oxPL/DPPC isotherms of the same compositions (Fig. 2, *A* and *B*). For all compositions and pressures the domains for PoxnoPC/DPPC are smaller and their number higher than for PazePC/DPPC (Fig. 5). The shape of the solid domains in oxPL/DPPC mixed monolayers is more uniform than those seen in neat DPPC and the domains remain stable and distinguishable also at high pressures of ~40–50 mN/m.

DISCUSSION

Because of the impairment of a number of cellular processes by lipid peroxidation (e.g., 41,43–45) it was of interest to characterize and compare the surface properties of the two oxidatively modified phospholipids PazePC and PoxnoPC, as reflected in their impact on mixed monolayers with DPPC. These two lipids were chosen for this study to be able to evaluate unambiguously the contribution of the aldehyde and carboxylic functions to their properties. Yet, our preliminary experiments with mixtures obtained from reacting 1-palmitoyl-2-linoleoyl-PC (PLPC) in the so-called Fenton reaction with H_2O_2 and $FeCl_2$ (K. Sabatini, F. M. Megli, and P. J. K.

FIGURE 2 (Continued).
mean molecular areas $\bar{A}$ versus X_{oxPL} for PoxnoPC and PazePC, respectively, as binary mixtures with DPPC at 5 (■), 10 (●), 20 (▲), 40 (▼), and 50 (♦) mN/m. The data were taken from the graphs in panels *A* and *B*. Standard deviations would be contained within the symbols and were omitted for the sake of clarity. Panels *E* and *F* compile the values for π versus elastic moduli C_s^{-1} calculated from panels *A* and *B*, for PoxnoPC and PazePC containing films, respectively, with increasing X_{oxPL} as (*a*) 0.0, (*b*) 0.5, (*c*) 0.25, and (*d*) 1.0. Corresponding C_s^{-1} versus X_{oxPC} data at 5 (■), 10 (●), 20 (▲), 40 (▼), and 50 (♦) mN/m, are shown for PoxnoPC/DPPC (*G*) and PazePC/DPPC (*H*) monolayers, and were taken from the graphs illustrated in panels *A* and *B*.

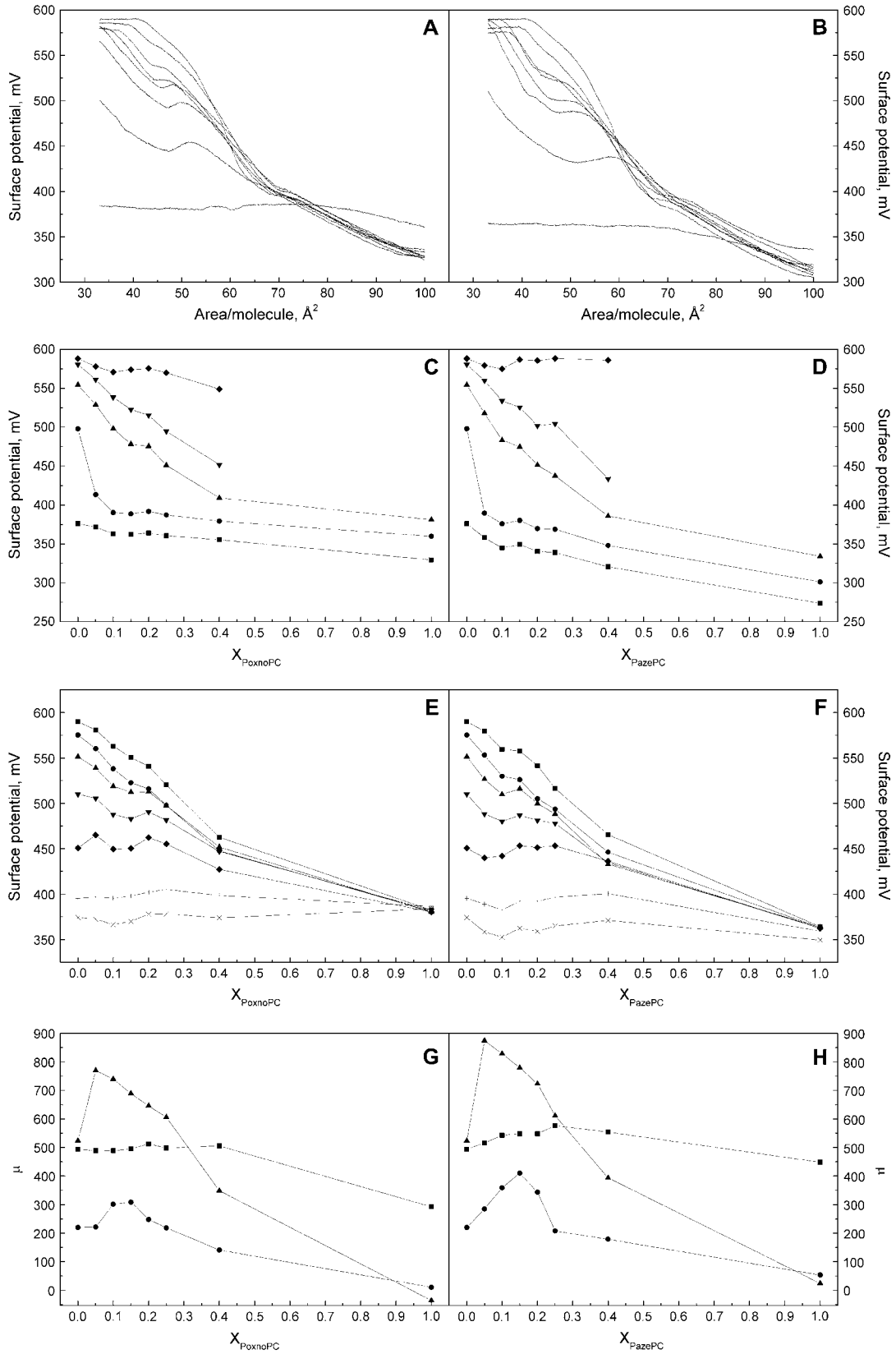

FIGURE 3 Representative surface potential $\Delta\psi$ versus $\bar{A}$ for PoxnoPC/DPPC (*A*) and PazePC/DPPC (*B*) monolayers. X_{oxPL} increases (*top to bottom*) from 0.0, 0.05, 0.1, 0.15, 0.2, 0.25, 0.4, to 1.0. Panels *C* and *D* depict isobars for $\Delta\psi$ versus X_{oxPL} data for PoxnoPC/DPPC and PazePC/DPPC films, respectively, at constant lateral pressure of 5 (■), 10 (●), 20 (▲), 40 (▼), and 50 (♦) mN/m. Panels *E* and *F* show isochores of $\Delta\psi$ versus X_{oxPL} for PoxnoPC and PazePC,

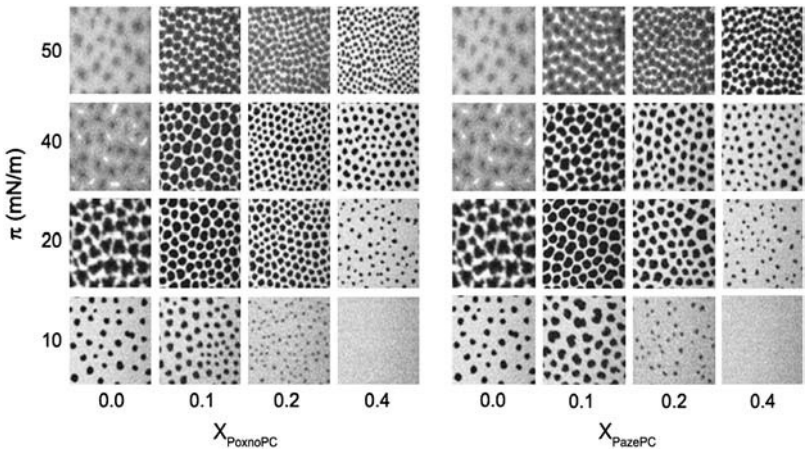

FIGURE 4 Fluorescence microscopy images for PoxnoPC/DPPC (*A*) and PazePC/DPPC (*B*) monolayers as a function of X_{oxPL} and recorded at the indicated values of π. All monolayers contained NBD-PC ($X = 0.01$) as the fluorescent dye. Compression rate was 2.5 Å^2/acyl chain/min and the subphase was 15 mM NaCl, pH 7.4. Images were recorded at ambient temperature of 24 ± 1°C.

Kinnunen, unpublished observations) revealed very similar overall behavior to what is reported here for the two pure oxidized phosphatidylcholines. Compared to neat DPPC the presence of the polar modifications of the *sn*-2 acyl chain in these oxPLs exerted drastic effects on the monolayer compression isotherms and film organization. In brief, both oxidized lipids expanded the monolayers and caused a gradual disappearance of the LC–LE coexistence region, together with the progressive appearance of a discontinuity at higher pressures, caused by the loss of oxPLs from the monolayer into the subphase. Further, both oxPLs lowered the monolayer surface potential considerably, together with the appearance of a local maximum coinciding with the onset of the high surface pressure transition. Importantly, the most pronounced modifications to monolayer electrical properties occurred in the surface pressure range of 20–40 mN/m, thus including equilibrium lateral pressure of ~33 mN/m estimated for natural membranes (61). Finally, evident from fluorescence microscopy, both PazePC and PoxnoPC in mixed monolayers with DPPC shift the appearance of LC domains to higher surface pressures.

To allow for rational analysis of the impact of these lipids, we needed to characterize their impact over the whole range of mol fractions, from 0 to 1.0. Unfortunately, as far as we are aware of, direct quantification of the various lipid peroxides from tissues has not been reported. Accordingly, the extent of lipid peroxidation is monitored indirectly based on the measurement of conjugated dienes, lipid hydroperoxides, isoprostanes, and degradation products such as malodialdehyde and 4-hydroxynoneal. These compounds represent steps in the radical chain reaction, some of them are unstable and susceptible to autooxidation and may additionally derive from reactions other than lipid peroxidation. The above factors make these assays prone to errors (38) and the quantitative assessment of the level of oxidative modifications remains a challenge. The oxidized PCs studied here represent oxidation products of one of the most abundant phospholipid of human membranes, 1-palmitoyl-2-oleyl-*sn*-glycero-3-phosphocholine (POPC), and are additionally derived from other common phosphatidylcholines bearing a *cis*-9 double bond containing fatty acid (e.g., palmitoleic, linoleic, or linolenic acid) in the *sn*-2 position. PoxnoPC has been recognized as the main product of ozone mediated oxidation of lung surfactant extract, possessing apoptosis and necrosis promoting activity (62). PazePC is present in low density lipoprotein (LDL) and has been shown to function as a weak ligand for the peroxisome proliferator-activated receptor, PPAR (63).

A model where the hydrophilic group bearing *sn*-2 acyl chains of PazePC and PoxnoPC would reverse their direction so as to accommodate the polar moieties into the vicinity of the lipid headgroups in the air-water interface (Fig. 6 *A*) could readily explain the expansion of the monolayer. This is in keeping with results of previous studies (48,64,65) revealing that oxidatively modified fatty acyl chains may locate closer to the interface than the corresponding unoxidized chains. Chain reversal is well established also for fluorescent phospholipid analogs bearing aromatic moieties in the *sn*-2 chain (e.g., 66). The similarities between the two oxidized lipids are rather striking. Yet, there were also distinct differences. Film expansion was more pronounced for PazePC, most likely reflecting its charge upon deprotonation of the carboxylic moiety, its higher affinity for water, and perhaps also the larger size compared to the aldehyde moiety of PoxnoPC, all the above features manifesting upon the looping back of the −COOH moiety into the lipid-water interfacial region. Coulombic repulsion between the negative charges of lipid headgroup phosphates and the deprotonated

FIGURE 3 (Continued).
respectively, constructed at constant mean molecular areas of 40 (■), 45 (●), 50 (▲), 55 (▼), 60 (♦), 70 (+), and 80 (×) Å^2/molecule. Also shown is $\mu\perp$ versus X_{oxPL} for PoxnoPC (*G*) and PazePC (*H*) containing films at 75–90 (corresponding to the liquid expanded phase), (■), 61–65 (▲), and 40–45 (●) Å^2/molecule.

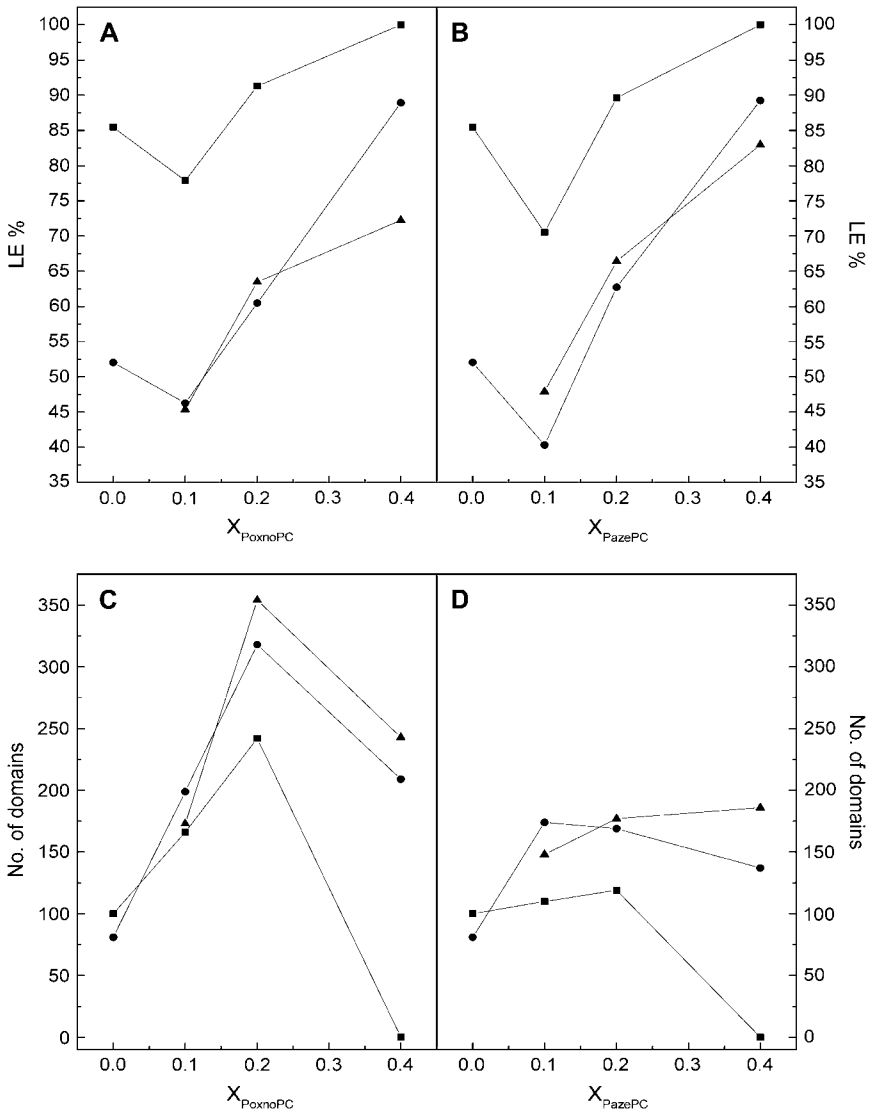

FIGURE 5 Percentage of the monolayer in the liquid expanded phase, %LE versus X_{oxPL} (*A* and *B*) and the number of domains for PoxnoPC/DPPC and PazePC/DPPC (*C* and *D*) at a constant lateral pressure of 10 (■), 20 (●), and 40 (▲) mN/m.

carboxylic moieties together with possible difference in the size of the hydration shell of the aldehyde and carboxylic groups could thus contribute to the difference in film expansion by PoxnoPC and PazePC, respectively. The above is in agreement with Phillips and Chapman (57), who demonstrated the expansion of PC and PE films to reflect the properties of their polar headgroups. Additionally, the orientation of the oxidatively modified *sn*-2 acyl chains suggested above leads to the accumulation of polar groups in the interfacial region, and hence to the reorganization of the intramolecular electric dipoles, including the P^{-}-N^{+}-dipoles of the PC headgroups of DPPC and oxPLs, explaining the decrease of the monolayer surface potential. Moreover, the disappearance of the LC-LE transition and a shift of the isotherms to the right (e.g., toward larger *A*/molecule) in the presence of oxPLs, indicate that the film is in the LE state (Fig. 2, *A* and *B*). It has been demonstrated that monolayer expansion depends on the length of the acyl chains (57), lipids with shorter chains forming more fluid and expanded monolayers. Analogously, the reversal of the oxidatively modified *sn*-2 acyl chains toward the interface decreases its effective length, thereby increasing the free volume available for the *sn*-1 chains, with their long axis remaining perpendicular to the membrane plane. Continuing this line of thought, one can also anticipate that at constant temperature and pressure the oxPL/DPPC mixed monolayers are less ordered compared to pure DPPC, complying with the disappearance of the LE-LC coexistence region and with the growth of the LE phase at $X_{oxPL} \geq 0.2$ (Fig. 5).

Importantly, acyl chain reversal alone is not enough to explain the presence of the shoulder at ~42 mN/m (Fig. 2, *A* and *B*) and the decrease of the area at collapse from ~40 to 25 $Å^2$/molecule with $X_{oxPL} = 0.40$. On the contrary, the area at collapse should increase because of the presence of the acyl chains bearing the polar group at the interface. Accordingly, in addition to the above process, reorientation

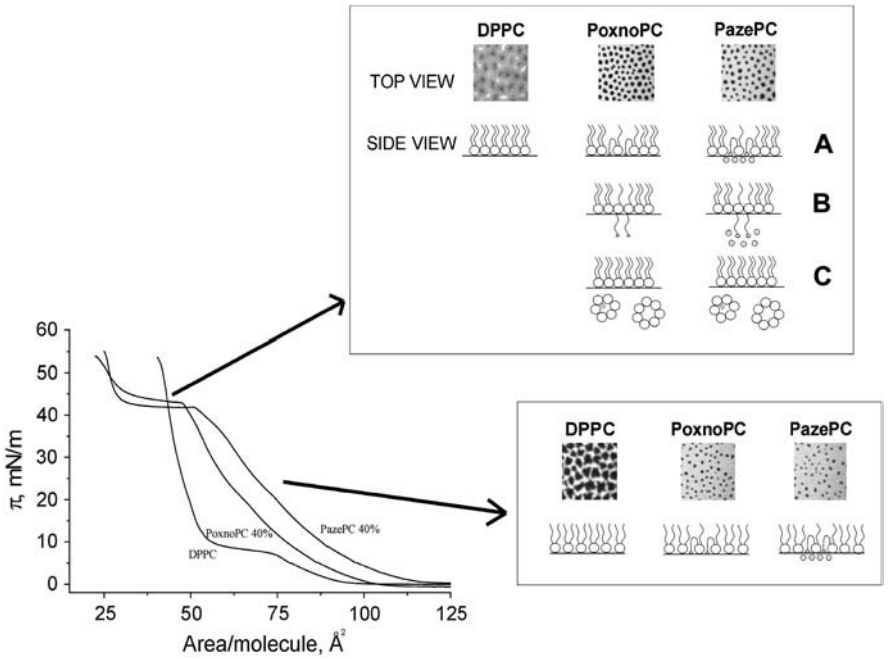

FIGURE 6 A schematic illustration of the possible arrangements of the *sn*-2 acyl chains of PazePC and PoxnoPC in DPPC during monolayer compression. See Discussion for details.

and complete extension of the modified *sn*-2 chains in the so-called extended lipid conformation (67) into aqueous phase (Fig. 6 *B*) followed by dissolving of the oxidized PLs into the aqueous subphase (Fig. 6 *C*) seems likely and could explain the presence of the above-mentioned shoulder in the compression isotherms. For the extended conformation the value of *A*/chain at collapse should be $\sim$(*A*/chain)/$1 - 0.5 \times X_{\mathrm{oxPL}}$, whereas upon loss of the oxidized phospholipids from the monolayer this should be (*A*/chain)/$1 - X_{\mathrm{oxPL}}$. For PoxnoPC/DPPC at $X_{\mathrm{PoxnoPC}} = 0.4$ (Fig. 2 *A*), the *A*/molecule at collapse is $\sim$23 Å^2, i.e., area/chain is $\sim$11.5 Å^2. Hence, for the extended conformation we get *A*/chain = (*A*/chain)/$1 - 0.5 \times 0.4$ = (*A*/chain)/0.8 = 11.5 Å^2/0.8 $\approx$ 14.4 Å^2, and upon loss of oxPL from the film *A*/chain = (*A*/chain)/$1 - 0.4$ = (*A*/chain)/0.6 $\approx$ 19.2 Å^2. The latter value is close to the amount of lipid present for pure DPPC at collapse, *A*/chain $\approx$ 20 Å^2. Dissolving of oxPLs from the monolayers and micelle formation, preceded by adoption of the extended conformation thus seems very likely. Notably, the same result is obtained by estimating the value of $A \approx 25$ Å^2 for $X_{\mathrm{PoxnoPC}} =$ 0.4 at 50 mN/m (Fig. 2 *C*). If we assume that all PoxnoPC dissolves into the aqueous subphase, we will have 60% of the applied lipid remaining in the film. Accordingly, (*A*/molecule)/$1 - X_{\mathrm{PoxnoPC}} = 25$ Å^2/0.6 $\approx$ 42 Å^2, which agrees exactly with the value of *A* for pure DPPC at 50 mN/m, $\approx$ 42 Å^2. Based on the above the condensing effect by oxPLs on DPPC monolayers at high lateral pressures appears to be apparent only and be caused by loss of the oxidatively modified lipids into the subphase, reducing the amount of total lipid in the monolayer. To this end, extrapolation of the $\bar{A}$ versus X_{oxPL} data at $\pi = 50$ mN/m (Fig. 2, *C* and *D*) to $X_{\mathrm{oxPL}} = 1.0$ approaches zero for both PazePC and PoxnoPC, revealing loss of the oxidized lipid from the monolayer. Finally, the fact that neat PoxnoPC and PazePC films collapse at pressures slightly lower than the values for π_s for the mixed films suggests that the regions where solubilization occurs are either binary mixtures of the oxPLs and DPPC, enriched in the former, or that they are very small so that the surrounding matrix may retain the departing oxPLs in the film.

Importantly, the extended conformation provides a rational explanation also for the changes in surface potential preceding the loss of oxPLs from the monolayer and in particular the negative slope of the associated shoulder, with the surface potential being affected by extension of the polar groups of the *sn*-2 chains into the aqueous phase. The value for *A*/molecule $\approx$ 34 Å^2 for PoxnoPC/DPPC with $X_{\mathrm{PoxnoPC}} =$ 0.4 at the film collapse corresponds to surface potential $\approx$ 500 mV (Fig. 3 *A*). Correcting this for X_{DPPC} we obtain 34 Å^2/0.6 $\approx$ 56.7 Å^2, which agrees well with the *A*/molecule = 56 Å^2 for pure DPPC at the same value of surface potential. Our surface potential data therefore support the conclusion that we are observing a biphasic process, in which the oxPLs in the DPPC matrix first adopt the extended conformation and subsequently dissolve into the subphase upon further increase in π. Interestingly, it has been observed that the ability of monolayers containing oxidized phospholipid species to accumulate the 42-residue form of amyloid β-protein (Aβ42) is attenuated at high surface pressures ($\pi > 35$ mN/m), presumably due to loss of interactions between the protein and functional groups of the oxPLs (68). Based on these findings this is likely to be caused by the loss of oxPLs from the monolayer diminishing the association of Aβ42 with the lipid film.

Phase separation seems feasible, with regions enriched in DPPC and PazePC or PoxnoPC being present, with the *sn*-2 acyl chains of the latter phospholipid sticking to the subphase. The model presented above, based on the surface pressure and surface potential measurements, is in agreement with our fluorescence microscopy results. Accordingly, for both PazePC and PoxnoPC the fluid phase remains at $\pi = 50$ mN/m, together with clearly distinguishable nonfluorescent solid domains. For pure DPPC the domain boundaries became blurred already below 40 mN/m and it is possible to distinguish four phases, viz. dark (LC), light gray to dark gray regions, and NBD-PC crystallized into clusters appearing as bright white spots (Fig. 4). Already low contents of PoxnoPC or PazePC ($X = 0.05$) caused the NBD-enriched domains to disappear. The prevalence of the fluid phase in the vicinity of the loss of oxPLs from the monolayers could involve lateral segregation of the oxPL molecules in the extended conformation. The diminished number and larger size of the domains evident in PazePC/DPPC monolayers compared to PoxnoPC/DPPC could arise from an attraction between the PazePC molecules in the extended conformation due to H-bonding between the acyl chains and between the latter and water molecules. Instead, compared to PazePC, PoxnoPC molecules seem to be more equally distributed in the monolayer leading to smaller and more numerous DPPC domains, indicating lower line tension between the DPPC enriched solid domains and the LE phase enriched PoxnoPC. Increase in the area of the liquid expanded phase in DPPC monolayers with $X_{\mathrm{oxPL}} > 0.1$ is evident upon examination of the fluorescence images (Fig. 5). However, at $X_{\mathrm{oxPL}} = 0.1$ there is a decrease in the percentage of the binary monolayer in the LE phase. Intriguingly, $\mu\perp$ goes through a sharp maximum at this film composition, its value then decreasing back to the level of pure DPPC at $X_{\mathrm{oxPL}} = 0.2$ (Fig. 3, *G* and *H*). Thus, between these X_{oxPL} values the reorientation of the headgroup P^{-}-N^{+} -dipoles could be possible. Subsequently, $\mu\perp$ decreases whereas the percentage of LE phase increases with increasing X_{oxPL}. This indicates that the phase state of DPPC monolayers is affected by the presence of oxPLs per se and depends on the content of these lipids in the monolayer, further modifying the orientation of the headgroup and the physical state of the matrix lipid. Finally, the packing density dependent changes in the orientation of the oxidatively modified chains readily implies phospholipids such as PoxoPC and PazePC to have profound effects on the lateral pressure profile as well the dielectricity gradient of bilayers, including augmented penetration of water into the hydrocarbon phase of the lipid. As a consequence, oxidation of membrane lipids should have dramatic impact on the assembly, conformation, and activity of membrane associated proteins.

The authors thank Prof. Howard L. Brockman and Dr. Juha-Matti Alakoskela for critical reading of the manuscript and Kaija Niva and Kristiina Söderholm for skillful technical assistance.

K.S. is supported by a fellowship from ESF (P.O.P 2000-2006). H.B.B.G. is supported by Finnish Academy, Marie Curie Training Network, COST D22, and Sigrid Jusèlius Foundation.

REFERENCES

1. Kinnunen, P. K. J. 1991. On the principles of functional ordering in biological membranes. *Chem. Phys. Lipids.* 57:375–399.
2. Kinnunen, P. K. J., A. Koiv, J. Y. A. Lehtonen, M. Rytömaa, and P. Mustonen. 1994. Lipid dynamics and peripheral interactions of proteins with membrane surfaces. *Chem. Phys. Lipids.* 73:181–207.
3. Mouritsen, O. G., and P. K. J. Kinnunen. 1996. Role of lipid organization and dynamics for membrane functionality. *In* Biological Membranes: A Molecular Perspective from Computation and Experiment. K. M. Merz Jr., and B. Roux, editors. Birkhäuser, Berlin. 463–502.
4. Mouritsen, O. G. 2005. Life as a Matter of Fat: The Emerging Science of Lipidomics. Springer-Verlag, Berlin Heidelberg.
5. Singer, S. J., and G. L. Nicolson. 1972. The fluid mosaic model of the structure of cell membranes. *Science.* 175:720–731.
6. Jacobson, K., E. D. Sheets, and R. Simson. 1995. Revisiting the fluid mosaic model of membranes. *Science.* 268:1441–1442.
7. Glaser, M. 1993. Lipid domains in biological membranes. *Curr. Opin. Struct. Biol.* 3:475–481.
8. Varma, R., and S. Mayor. 1998. GPI-anchored proteins are organized in submicron domains at the cell surface. *Nature.* 394:798–801.
9. Hwang, J., L. A. Gheber, L. Margolis, and M. Edidin. 1998. Domains in cell plasma membrane investigated by near-field scanning optical microscopy. *Biophys. J.* 74:2184–2190.
10. Gutierrez Merino, C. 1987. Gel to liquid crystalline phase transition promotes a conformational reorganization of Ca+, Mg2+-ATPase from sarcoplasmic reticulum in dimyristoylphosphatidylcoline reconstituted system. *Arch. Biochem. Biophys.* 252:303–314.
11. Welti, R., and M. Glaser. 1994. Lipid domains in model and biological membranes. *Chem. Phys. Lipids.* 73:121–137.
12. Lehtonen, J. Y. A., and P. K. J. Kinnunen. 1995. Phospholipase A2 as a mechanosensor. *Biophys. J.* 68:1888–1894.
13. Karlsson, O., M. Rytömaa, A. Dahlqvist, P. K. J. Kinnunen, and Å. Wieslander. 1996. Correlation between bilayer lipid dynamics and activity of the diglucosyldiacylglycerol synthase from Acholeplasma laidlawii membranes. *Biochemistry.* 35:10094–10102.
14. Prenner, E., A. Sommer, N. Maurer, O. Glatter, R. Gorges, F. Paltauf, and A. Hermetter. 2000. Lateral microheterogeneity of diphenylhexatriene-labeled choline phospholipids in the erythrocyte ghost membrane as determined by time-resolved fluorescence spectroscopy. *J. Membr. Biol.* 174:237–243.
15. Schutz, G. J., G. Kada, V. P. Pastuushenko, and H. Schindler. 2000. Properties of lipid microdomains in a muscle cell membrane visualized by single molecule microscopy. *EMBO J.* 19:892–901.
16. Storm, P., L. Li, P. K. J. Kinnunen, and Å. Wieslander. 2003. Lateral organization in Acholeplasma laidlawii lipid bilayer models containing endogenous pyrene probes. *Eur. J. Biochem.* 270:1699–1709.
17. Lee, A. G. 2004. How lipids affect the activities of integral membrane proteins. *Biochim. Biophys. Acta.* 1666:62–87.
18. Jensen, M. O., and O. G. Mouritsen. 2004. Lipids do influence protein function - the hydrophobic matching hypothesis revisited. *Biochim. Biophys. Acta.* 1666:205–226.
19. Mustonen, P., J. A. Virtanen, P. J. Somerharju, and P. K. J. Kinnunen. 1987. Binding of cytochrome c to liposomes as revealed by the quenching of fluorescence from pyrene-labeled phospholipids. *Biochemistry.* 26:2991–2997.
20. Tuominen, E. K., C. J. Wallace, and P. K. J. Kinnunen. 2002. Phospholipid-cytochrome c interaction: evidence for the extended lipid anchorage. *J. Biol. Chem.* 277:8822–8826.

21. Halliwell, B., and J. M. Gutteridge. 1990. Role of free radicals and catalytic metal ions in human disease: an overview. *Methods Enzymol.* 186: 1–85.

22. Kinnunen, P. K. J. 2000. Lipid bilayers as osmotic response elements. *Cell. Physiol. Biochem.* 10:234–250.

23. Killian, J. A. 2003. Synthetic peptides as models for intrinsic membrane proteins. *FEBS Lett.* 555:134–138.

24. Killian, J. A., and G. von Heijne. 2000. How proteins adapt to a membrane-water interface. *Trends Biochem. Sci.* 25:429–434.

25. Lee, A. G. 2003. Lipid-protein interactions in biological membranes: a structural perspective. *Biochim. Biophys. Acta.* 1621:1–40.

26. Valyi-Nagy, T., and T. S. Dermody. 2005. Role of oxidative damage in the pathogenesis of viral infections of the nervous system. *Histol. Histopathol.* 20:957–967.

27. Wood, L. G., P. G. Gibson, and M. L. Garg. 2003. Biomarkers of lipid peroxidation, airway inflammation and asthma. *Eur. Respir. J.* 21:177–186.

28. Ames, B. N., M. K. Shigenaga, and T. M. Hagen. 1993. Oxidants, antioxidants, and the degenerative diseases of aging. *Proc. Natl. Acad. Sci. USA.* 90:7915–7922.

29. Beckman, J. S., and W. H. Koppenol. 1996. Nitric oxide, superoxide, and peroxynitrite: the good, the bad, the ugly. *Am. J. Physiol. Cell Physiol.* 271:1424–1437.

30. Demple, B., and L. Harrison. 1994. Repair of oxidative damage to DNA: enzymology and biology. *Annu. Rev. Biochem.* 63:915–948.

31. Halliwell, B. 1989. Oxidants and the central nervous system: some fundamental question. Is oxidant damage relevant to Parkinson's disease, Alzheimer's disease, traumatic injury or stroke? *Acta Neurol. Scand. Suppl.* 126:23–33.

32. Butterfield, D. A., J. Drake, C. Pocernich, and A. Castegna. 2001. Evidence of oxidative damage in Alzheimer's disease brain: central role for amyloid beta-peptide. *Trends Mol. Med.* 7:548–554.

33. Everse, J., and P. W. Coates. 2005. Role of peroxidases in Parkinson disease: a hypothesis. *Free Radic. Biol. Med.* 38:1296–1310.

34. Berg, D., M. B. Youdim, and P. Riederer. 2004. Redox imbalance. *Cell Tissue Res.* 318:201–213.

35. Berliner, J. A., and J. W. Heinecke. 1996. The role of oxidized lipoproteins in atherogenesis. *Free Radic. Biol. Med.* 20:707–727.

36. Zhang, X. Y., Y. L. Tan, L. Y. Cao, G. Y. Wu, O. Xu, Y. Shen, and D. F. Zhou. 2006. Antioxidant enzymes and lipid peroxidation in different forms of schizophrenia treated with typical and atypical antipsychotics. *Schizophr. Res.* 81:291–300

37. Hu, W., Z. Feng, J. Eveleigh, G. Iyer, J. Pan, S. Amin, F. Chung, and M. Tang. 2002. The major lipid peroxidation product, trans-4-hydroxy-2-nonenal, preferentially forms DNA adducts at codon 249 of human p53 gene, a unique mutational hotspot in hepatocellular carcinoma. *Carcinogenesis.* 23:1781–1789.

38. Gago-Dominguez, M., J. E. Castelao, J. M. Yuan, R. K. Ross, and M. C. Yu. 2002. Lipid peroxidation: a novel and unifying concept of the etiology of renal cell carcinoma (United States). *Cancer Causes Control.* 13:287–293.

39. Sander, C. S., F. Hamm, P. Elsner, and J. J. Thiele. 2003. Oxidative stress in malignant melanoma and non-melanoma skin cancer. *Br. J. Dermatol.* 148:913–922.

40. Cejas, P., E. Casado, C. Belda-Iniesta, J. De Castro, E. Espinosa, A. Redondo, M. Sereno, M. A. Garcia-Cabezas, J. A. F. Vara, A. Domínguez-Caceres, R. Perona, and M. Gonzales-Baron. 2004. Implication of oxidative stress and cell membrane lipid peroxidation in human cancer (Spain). *Cancer Causes Control.* 15:707–719.

41. Kourie, J. I. 1998. Interaction of reactive oxygen species with ion transport mechanism. *Am. J. Physiol. Cell Physiol.* 275:C1–C24.

42. Kinnunen, P. K. J. 1996. On the molecular-level mechanism of peripheral protein-membrane interactions induced by lipids forming inverted non-lamellar phases. *Chem. Phys. Lipids.* 81:151–166.

43. Gabbita, S. P., D. A. Butterfield, K. Hensley, W. Shaw, and J. M. Carney. 1997. Aging and caloric restriction affect mitochondrial respiration and lipid membrane status: an electron paramagnetic resonance investigation. *Free Radic. Biol. Med.* 23:191–201.

44. Gabbita, S. P., R. Subramaniam, F. Allouch, J. M. Carney, and D. A. Butterfield. 1998. Effects of mitochondrial respiratory stimulation on membrane lipids and proteins: an electron paramagnetic resonance investigation. *Biochim. Biophys. Acta.* 1372:163–173.

45. Nepomuceno, M. F., A. Alonso, L. Pereira-Da-Silva, and M. Tabak. 1997. Inhibitory effect of dipyridamole and its derivatives on lipid peroxidation in mitochondria. *Free Radic. Biol. Med.* 23:1046–1054.

46. Smith, I. C. P., and K. W. Butler. 1976. Oriented lipid systems as model membranes. *In* Spin Labeling Theory and Applications. L. J. Berliner, editor. Academic Press, New York. 411–451.

47. Jost, P., L. J. Libertini, V. C. Hebert, and O. H. Griffith. 1971. Lipid spin labels in lecithin multilayers. A study of motion along fatty acid chains. *J. Mol. Biol.* 59:77–98.

48. Megli, F. M., and K. Sabatini. 2003a. EPR studies of phospholipid bilayer after lipoperoxidation. 1. Inner molecular order and fluidity gradient. *Chem. Phys. Lipids.* 125:161–172.

49. Megli, F. M., and K. Sabatini. 2003b. Respiration state IV-generated ROS destroy the mitochondrial bilayer packing order in vitro. An EPR study. *FEBS Lett.* 550:185–189.

50. Megli, F. M., and K. Sabatini. 2004. Mitochondrial phospholipid bilayer structure is ruined after liver oxidative injury in vivo. *FEBS Lett.* 573:68–72.

51. Gago-Dominguez, M., J. E. Castelao, M. C. Pike, A. Sevanian, and R. W. Haile. 2005. Role of lipid peroxidation in the epidemiology and prevention of breast cancer. *Cancer Epidemiol. Biomarkers Prev.* 14: 2829–2839.

52. Brockman, H. L. 1999. Lipid monolayers: why use half membrane to characterize protein-membrane interaction? *Curr. Opin. Struct. Biol.* 9:438–443.

53. Brockman, H. L. 1994. Dipole potential of lipid membranes. *Chem. Phys. Lipids.* 73:57–79.

54. Brockman, H. L., C. M. Jones, C. J. Schwebke, J. M. Smaby, and D. E. Jarvis. 1980. Application of a microcomputer-controlled film balance system to collection and analysis of data from mixed monolayers. *J. Colloid Interface Sci.* 78:502–512.

55. Smaby, J. M., V. S. Kulkarni, M. Momsen, and R. E. Brown. 1996. The interfacial elastic packing interactions of galactosylceramides, sphingomyelins, and phosphatidylcholines. *Biophys. J.* 70: 868–877.

56. Weis, R. M. 1991. Fluorescence microscopy of phospholipid monolayer phase transitions. *Chem. Phys. Lipids.* 57:227–239.

57. Phillips, M. C., and D. Chapman. 1968. Monolayer characteristics of saturated 1,2-diacyl phosphatidylcholines (lecithins) and phosphatidylethanolamines at the air-water interface. *Biochim. Biophys. Acta.* 163:301–313.

58. Megli, F. M., L. Russo, and K. Sabatini. 2005. Oxidized phospholipids induce phase separation in lipid vescicles. *FEBS Lett.* 579:4577–4584.

59. Lösche, M., E. Sackmann, and H. Möhwald. 1983. A fluorescence microscopic study concerning the phase diagram of phospholipids. *Ber. Bunsen-Ges. Phys. Chem.* 87:848–852.

60. McConnell, H. M., L. K. Tamm, and R. M. Weis. 1984. Periodic structures in lipid monolayer phase transitions. *Proc. Natl. Acad. Sci. USA.* 81:3249–3253.

61. Demel, R. A., W. S. Geurts van Kessel, R. F. Zwaal, B. Roelofsen, and L. L. van Deenen. 1975. Relation between various phospholipase actions on human red cell membranes and the interfacial phospholipid pressure in monolayers. *Biochim. Biophys. Acta.* 406:97–107.

62. Uhlson, C., K. Harrison, C. B. Allen, S. Ahmad, C. W. White, and R. C. Murphy. 2002. Oxidized phospholipids derived from ozone-treated lung surfactant extract reduce macrophage and epithelial cell viability. *Chem. Res. Toxicol.* 15:896–906.

63. Davies, S. S., A. V. Pontsler, G. K. Marathe, K. A. Harrison, R. C. Murphy, J. C. Hinshaw, G. D. Prestwich, A. St. Hilaire, S. M. Prescott, G. A. Zimmerman, and T. M. McIntyre. 2001. Oxidized alkyl

phospholipids are specific, high affinity peroxisome proliferator-activated receptor γ ligands and agonists. *J. Biol. Chem.* 276:16015–16023.

64. van Kuijk, F. J. G. M., A. Sevanian, G. Handelman, and E. A. Dratz. 1988. A new role for phospholipase A2: protection of membranes from lipid peroxidation damage. *Trends Biochem. Sci.* 12:31–34.
65. Wratten, M. L., G. van Ginkel, A. A. van'tVeld, A. Bekker, E. E. van Faassen, and A. Sevanian. 1992. Structural and dynamic effects of oxidatively modified phospholipids in unsaturated lipid membranes. *Biochemistry.* 31:10901–10907.
66. Alakoskela, J. M., and P. K. Kinnunen. 2001. Control of a redox reaction on lipid bilayer surfaces by membrane dipole potential. *Biophys. J.* 80:294–304.
67. Kinnunen, P. K. J. 1992. Fusion of lipid bilayers: a model involving mechanistic connection to HII phase forming lipids. *Chem. Phys. Lipids.* 63:251–258.
68. Koppaka, V., and P. H. Axelsen. 2000. Accelerated accumulation of amyloid β proteins on oxidatively damaged lipid membranes. *Biochemistry.* 39:10011–10016.